First-principles studies of NO chemisorption on rhodium, palladium, and platinum surfaces

M.-H. Tsai* and K. C. Hass
Physics Department, Ford Motor Company, Scientific Research Laboratories, MD-3028, Dearborn, Michigan 48121-2053
(Received 1 December 1994)

We examine the interactions between NO and the (100) surfaces of Rh, Pd, and Pt using the first-principles pseudofunction method for slab geometries. This all-electron, full-potential, local-density-approximation (LDA) approach is applied here to clean metal surfaces, free-standing NO monolayers, and half-monolayer chemisorbed systems with NO linearly bonded in twofold bridge and atop sites. The predicted clean metal surface electronic structures agree well with previous LDA results. Calculated total energies for NO monolayers yield an equilibrium bond length and N-O stretch frequency at large NO-NO distances close to experimental values for isolated molecules. The electronic structures and N—O bond lengths of the chemisorbed systems are similar for all three metals but show significant differences between bridge and atop geometries. NO-induced states in the former case agree well with photoemission and inverse photoemission data. On each metal, the bridge site is energetically favorable, with the atop site becoming increasingly disfavored in the order of Pt→Rh→Pd. This and related trends in N-O and metal-N stretch frequencies are attributed to differences in bulk metal properties. Bridge-site adsorption causes the N—O bond to lengthen and soften. Difficulties in interpreting adsorbate vibrational spectra on metal surfaces are emphasized.

I. INTRODUCTION

Rhodium, palladium, and platinum are the usual active ingredients in automotive catalysts.[1,2] So-called three-way catalysts, together with electronic control of engine air/fuel ratios, allow recently manufactured automobiles in the U.S. to meet stringent regulations on the emission of the three polutants CO, hydrocarbons, and NO_x. The simultaneous abatement of these three species is a remarkable technological achievement given that it requires the oxidation of CO and hydrocarbons and the reduction of NO_x. Since the mid-1970s, it has been known that Rh is particularly well suited for catalyzing NO_x reduction in three-way catalysts.[3] This realization has stimulated a great deal of interest in the fundamental surface science of NO interacting with Rh and other metals. While much has been learned from the extensive literature that has developed,[4] the key reasons for the effectiveness of Rh in automotive catalysis have still not been clearly identified.[5]

To date, most theoretical work on NO chemisorption on metal surfaces has been based on cluster models containing small numbers of metal atoms.[6–12] Such models do not correctly describe the continuum of metal states and the existence of a Fermi level at an extended metal surface. Consequently, they often do not provide a realistic picture of bonding to solid surfaces[13,14] or to larger clusters (10–100 Å) found in supported metal catalysts. The only computational method that has been extensively applied to NO on semi-infinite crystals is extended Hückel theory (EHT), as practiced by Hoffmann and coworkers.[15–18] These studies have yielded many important insights into NO chemisorption, and have recently suggested that NO reduction on Rh may involve an initial coupling to produce N_2O_2 dimers.[17,18] This is an interesting alternative to the more traditional view that NO reduction begins with NO dissociation.[19,20] It is well known, of course, that EHT is very approximate,[21] and there are many examples where its predictions have been superseded by those of more sophisticated calculations.[22] With this in mind, we have chosen to reexamine the molecular adsorption of NO on extended Rh, Pd, and Pt surfaces using a more reliable, first-principles approach.

The method we use is a slightly modified version of the all-electron, full-potential pseudofunction (PSF) method, as implemented for two-dimensional periodic slab geometries.[23,24] Exchange and correlation effects are treated within the local-density approximation (LDA) to density-functional theory.[25] The PSF method differs from but has similarities to the linearized-muffin-tin-orbital[26] (LMTO), linearized-augmented-plane-wave[26] (LAPW), and *ab initio* pseudopotential[27] methods. The PSF method has been extensively tested on a wide variety of covalent,[28] ionic,[29] and metallic[30] systems. It was originally developed for problems involving molecules on metal surfaces, such as that considered here, and it is particularly well suited for this task.[23,24]

To narrow the scope of this study, we focus on the (100) surfaces of Rh, Pd, and Pt, and consider the case of a half-monolayer coverage ($\theta=0.5$) of NO. The (100) surface is a convenient choice because it is intermediate in packing density between the close-packed (111) and the more open (110), and it was used in previous EHT studies of NO chemisorption in Refs. 16 and 17. The requirement of two-dimensional periodicity makes the present method computationally tractable only for relatively high coverages. Rh(100) and Pd(100) are saturated by NO at $\theta\approx0.67$.[31,32] A half-monolayer coverage is thus physically realizable but still high enough that it requires only a doubling of the two-dimensional unit cell compared to that of a clean metal surface. For simplicity, we consider only the cases of linear NO in twofold bridge and atop

sites. The possibility that NO tends to bend, as has been suggested by variational spectra on many metal surfaces,[4] including Pt(100),[33] would be tedious to address with the existing PSF method because of its inability to calculate forces on individual atoms.

Computational aspects of this work are described in Sec. II. Results for clean Rh, Pd, and Pt (100) surfaces are discussed in Sec. III. The hypothetical case of free-standing NO monolayers is examined in Sec. IV to isolate the effects of NO-NO interactions, which are significant in chemisorbed systems at high coverages. Results for coupled NO-metal systems are presented in Sec. V. The significance of this work is discussed further in Sec. VI.

II. COMPUTATIONAL DETAILS

Like the LMTO method,[26] the PSF formalism[23,24] employs atom-centered, localized basis functions which are derived from linearized solutions of the Schrödinger equation within muffin-tin spheres. The pseudofunctions themselves are spherical Hankel or Neumann tailing functions in the interstitial region, with smooth extensions into the muffin-tin regions. The spirit of this construction is similar to that of smooth pseudopotentials.[27] PSF basis orbitals are constructed by augmenting the smooth PSF's with appropriate linearized orbitals inside the muffin-tin spheres. In the original PSF method, this procedure was carried out by decomposing Fourier series of Bloch sums of PSF's into partial waves.[23,24] Here we use a slightly modified approach[34] based on calculated structure factors[35,36] for the spherical Hankel and Neumann functions. The PSF's are still expanded in Fourier series, but the number of plane waves required for convergence is reduced compared to the original method.

By taking into account the full variation in the potential in the interstitial region and the nonspherical variation inside each sphere, the PSF method achieves nearly the same accuracy as the full-potential LAPW method.[37] It is noteworthy, for example, that the PSF method yields excellent results for bulk Si without resorting to empty spheres.[28] The computational cost of the PSF method is comparable to that of LMTO since both use small basis sets. The combined accuracy and efficiency of the PSF method make it particularly useful for studying chemisorption, where the simultaneous presence of short molecular bonds and relatively large unit cells pose significant computational challenges.[23,24]

For Rh, Pd, and Pt, we use a basis of nine *s-p-d* orbitals with a decaying tail and four *s-p* orbitals with an oscillating tail. For N and O, we use a similar basis with the *d* orbitals excluded. Energy parameters for the decaying and oscillating tails are assumed to be -0.3 and $+0.5$ Ry, respectively. The results are not particularly sensitive to these values, which are based on previous experience.[28–30] Only in the case of atop-site adsorption do we raise both of these energy parameters slightly to reflect a noticeable increase in interstitial charge compared to that found for bridge-site adsorption.

The choice of muffin-tin radii is also somewhat arbitrary, although there is a strict requirement that the spheres do not overlap. Here we use $r_{MT}=2.54$, 2.59, 2.62, 1.00, and 1.00 a.u. for Rh, Pd, Pt, N, and O, respectively. To avoid overlap in calculations involving NO adsorbates, r_{MT} is reduced by about 10% for surface metal atoms. The maximum wave-vector components ($\alpha=x$, y, and z) for plane-wave expansions of PSF's are determined by $G_\alpha \sim 7/r_{MT}$ for pure metals and $G_\alpha \sim 5/r_{MT}(N)$ for all systems containing NO.[38]

The PSF method is implemented for slab geometries by treating the vacuum regions as in Refs. 23 and 24. We model the (100) surfaces of Rh, Pd, and Pt using three-layered slabs. This number of layers is large enough to provide reasonable results for face-centered-cubic metals[15–17] but not so large as to make the cost of this study prohibitive. In all cases, we assume the metal atoms to be frozen in their truncated bulk lattice positions, with nearest-neighbor separations of 2.689, 2.750, and 2.774 Å, respectively, for Rh, Pd, and Pt.[39] Low-energy-electron-diffraction (LEED) experiments confirm that Rh(100) and Pd(100) are unreconstructed,[40,41] but find a 5×20 structure to be most stable on Pt(100).[33] The 1×1 Pt(100) surface studied here is also experimentally observable under certain conditions, particularly with adsorbates present.[33,40] The possibility that Rh(100) and Pd(100) may actually exhibit small ($<3\%$) anomalous outward relaxations[41,42] is not considered here, although it is currently of great interest.[43–46] Speculations on the origin of this effect include the possibilities of undetected adsorbates[43] and surface magnetism.[44]

NO chemisorption is modeled by adding NO molecules perpendicular to one of the outer layers of the three-layer metal slabs in either of the two $p(2\times1)$ adsorption geometries for $\theta=0.5$ shown in Fig. 1. Previous EHT studies have found the symmetry of the overlayer to be a relatively insignificant factor.[16] The alternative $c(2\times2)$ geometries also shown in Fig. 1 have been observed under certain conditions in LEED studies of NO/Rh(100) (Ref. 40) and NO/Pd(100).[47] We prefer to focus on the $p(2\times1)$ case because of its smaller NO-NO separation, which increases the competition between metal—NO bonding and NO—NO bonding.

The LDA exchange-correlation functional used in this work is that of Hedin and Lundquist.[25] A companion local-spin-density approximation[48] study shows that the

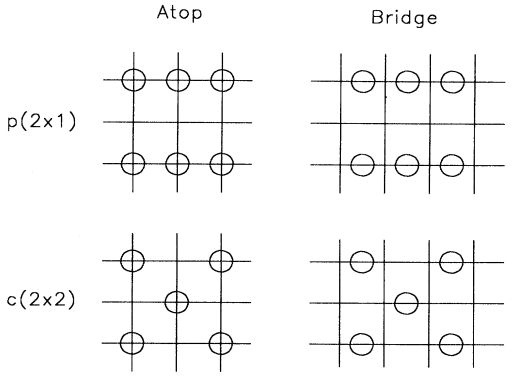

FIG. 1. Adsorption sites (circles) for a half-monolayer coverage of NO on a (100) surface, as viewed from above. Surface atoms lie at intersections.

neglect of explicit spin effects is reasonable in the present systems, despite the existence of an unpaired electron on NO itself.[49] All of the present calculations include scalar-relativistic corrections, which are essential for the heavy 5*d* element Pt and significant for the 4*d* elements Rh and Pd. Four special *k* points[50] in the two-dimensional irreducible Brillouin zones for slabs with 2×1 unit cells were used to achieve total-energy convergence to within 1 mRy. This convergence was often very slow due to charge sloshing, and was accelerated considerably by the procedure of Johnson.[51] Once a converged potential was obtained, as many as 23 *k* points were used to calculate charge densities, densities of states, and work functions.

III. CLEAN METAL SURFACES

The calculated electronic structures for the three-layer slab models reveal distinct differences between clean Rh, Pd, and Pt (100) surfaces. Figure 2 shows the PSF total densities of states for these systems on the same absolute energy scale, with the potential infinitely far from each slab set to zero. The vertical dashed lines denote the Fermi levels, which decrease in the series Rh→Pd→Pt. In each case, the Fermi level lies near the top of a high density of states region associated with *d* orbitals. The *d* bandwidth increases from about 5 eV in Pd to 6.5 eV in Rh to nearly 7 eV in Pt. These bandwidths are in the same order as in the bulk metals,[52–54] but are consistently smaller than the bulk values because of the lower coordination at the surface. The Rh and Pd spectra in Fig. 2 agree well with previous first-principles results for seven-layer slabs,[55–58] with the slight differences explainable in terms of the larger percentage of surface atoms in the three-layer case. By contrast, the present results sharply disagree with recent semiempirical EHT predictions for three-layer slabs;[17] that study yielded a larger bandwidth for Rh compared to Pt, and a higher Fermi level for Pt compared to Pd (see below).

The trends in Fig. 2, which we believe to be correct, are understandable in terms of the atomic properties of Rh, Pd, and Pt. Figure 3 shows the relative placement of these elements in the Periodic Table, together with their atomic numbers, ground-state electronic configurations, and *d*-orbital radii.[59] Rh has one fewer valence electron than Pd and Pt, which places the Rh Fermi level in Fig. 2 lower in the *d* band. The decrease in *d*-orbital radius and the corresponding downshift in *d*-orbital energies from Rh to Pd are typical of the trend across most of the 3*d*, 4*d*, and 5*d* transition series.[21,59] With increasing atomic number, the *d* orbitals are more strongly attracted to the nucleus because the additional nuclear charge is inefficiently shielded by additional *d* electrons. Since the states near the top of the *d* band are primarily antibonding in character, the extra electron in Pd compared to Rh also weakens the bonding and causes the lattice to expand. This further localizes the Pd *d* orbitals and gives rise to a very narrow *d* band. Pt, on the other hand, has a very broad *d* band because it has nearly the same lattice constant as Pd but a much larger *d* radius. The expansion of the *d* shell and the different atomic ground-state configuration of Pt compared to Pd results from its more relativistic nature. Relativistic effects are largest near the nucleus, and preferentially lower the energies of valence *s* and *p* states relative to *d* states.[60] This effect carries over to extended systems and results in a smaller effective *d*-orbital population in Pt compared to Pd in analogous

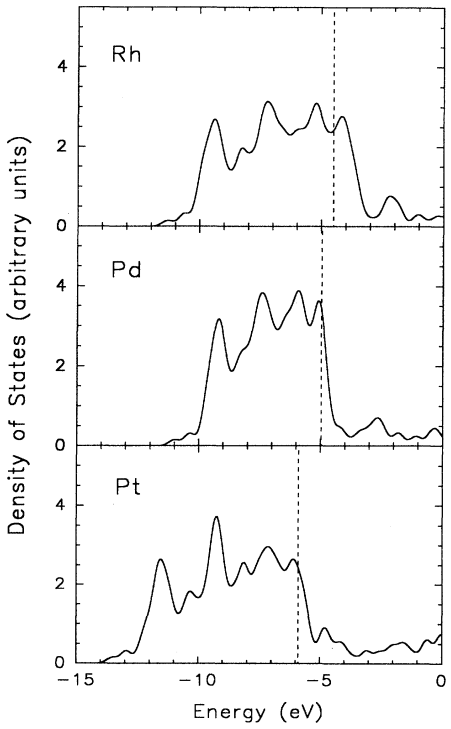

FIG. 2. Calculated total densities of states for three-layer slabs of Rh, Pd, and Pt with (100) surfaces. In each case the energy zero is the potential at infinity, and the Fermi level is denoted by a vertical dashed line. The results are broadened by 0.2 eV.

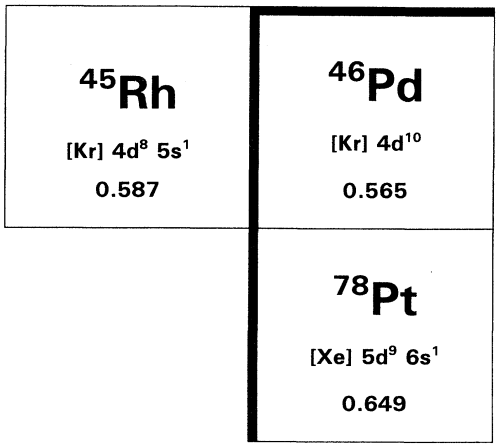

FIG. 3. Portion of the Periodic Table showing atomic numbers, ground-state electronic configurations, and *d*-orbital radii (in Å) for Rh, Pd, and Pt. The thick lines denote boundaries between dissociative (left) and molecular (right) chemisorption of NO at room temperature (from Ref. 70).

bonding environments (e.g., 8.75 vs 8.95 for bulk metals[54]).

The difference between Pd and Pt is further illustrated in Fig. 4, which shows calculated valence charge-density contours for one half of the three-layer slabs. The greater localization of d charge in Pd is apparent from the fact that the second highest level contour plotted completely encloses a Pd site, but contributes to a bridge between nearest-neighbor atoms in Pt. The larger bond charge in Pt reflects stronger interatomic bonding, which results from the slightly lower filling of antibonding d states. The more delocalized Pt charge also spreads more into the tetrahedral (T) and octahedral (O) interstitial regions and produces greater Smoluchowski smoothing at the surface.[61,62] The corresponding charge density for Rh (not shown here, but see Refs. 55 and 58) is very similar in appearance to that of Pt.

The absolute Fermi-level positions in Fig. 2 provide theoretical predictions for the metal (100) work functions. These results are compared in Table I to previously published theoretical[17,18,55–57,63] and experimental[64–67] values. The first three columns, which contain self-consistent local orbital (SCLO),[55,56] LAPW,[57] and LMTO (Ref. 63) results, respectively, are all based on LDA calculations for seven-layer (100) slabs. Scalar-relativistic effects were included only in the LAPW Rh and LMTO Pt calculations. Additional LAPW calculations for Rh slabs as thin as two layers[68] gave the same value as in the table to within 0.1 eV. The present PSF results agree reasonably well with these earlier LDA calculations, and are within the likely experimental uncertainties. With the exception of the EHT results already discussed,[17,18] all of the results in Table I agree that the work function increases in the series Rh→Pd→Pt. The large quantitative errors and incorrect ordering of Pd and Pt work functions in the EHT method are due primarily to the non-self-consistent nature of this approach and its associated neglect of surface dipole effects.[69]

The relative ordering of Fermi levels at different metal surfaces is an important factor in determining the trends in adsorbate bonding.[21] Ward, Hoffmann, and Shelef argued that NO chemisorption on Rh results in a weaker NO bond than on Pd or Pt because Rh has the highest Fermi level of the three metals.[17] The present results do not support this simple conclusion, although it is observed experimentally[70] that NO adsorbs dissociatively on Rh at room temperature, but molecularly on Pd and Pt. A portion of the dividing line in the Periodic Table between these two modes of behavior[70] is shown in bold in Fig. 3.

TABLE I. Comparisons of calculated and experimental work functions (in eV) for the (100) surfaces of Rh, Pd, and Pt.

	SCLO	LAPW	LMTO[a]	EHT[b]	This work	Expt.
Rh	4.8[c]	5.5[d]	5.24	8.62	4.51	4.6,[e] 4.98,[f] 5.2[g]
Pd	5.0[h]		5.30	10.97	4.96	5.12,[f] 5.3[i]
Pt			6.11	9.76	5.89	5.65[f]

[a]Reference 63.
[b]References 17 and 18.
[c]Reference 55.
[d]Reference 57.
[e]Reference 64.
[f]Polycrystalline value, from Ref. 65.
[g]Reference 66.
[h]Reference 56.
[i]Reference 67.

Many other aspects of the electronic structure of a metal surface are also important for understanding the chemisorption of a molecule like NO. Particularly relevant is the d-orbital decomposition of the surface layer density of states.[21,71] LMTO results for this decomposition for Rh and Pd (100) surfaces were recently discussed at length in Ref. 72, so we will not present our own similar PSF results here. Suffice it to say that the unoccupied d states are primarily of x^2-y^2 symmetry (with x and y the nearest-neighbor directions in the surface plane) in Pd and Pt, and of more mixed character in Rh.

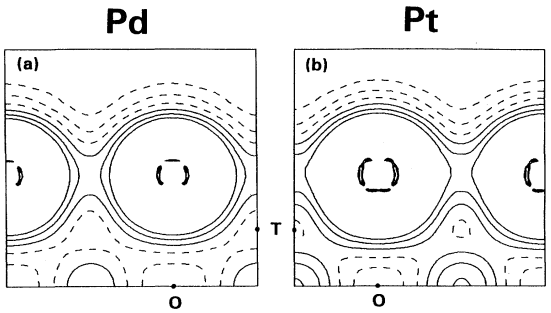

FIG. 4. Valence electronic charge densities for three-layer (a) Pd(100) and (b) Pt(100) slabs plotted on a plane perpendicular to the surface and passing through nearest-neighbor surface atoms. Dashed contours denote charge densities of 0.01, 0.02, and 0.03 a.u., and solid contours denote charge densities of 0.04, 0.05, and 0.06 a.u. T and O denote tetrahedral and octahedral interstitial sites, respectively.

IV. FREE-STANDING NO MONOLAYERS

To understand NO chemisorption at high coverages, it is useful first to examine the properties of free-standing NO monolayers. Figure 5 summarizes the results of PSF total-energy calculations for a variety of two-dimensional NO layers with both square (1×1) and rectangular (2×1) unit cells. In all cases, every NO molecule is aligned the same way perpendicular to the layer. The abscissa in Fig. 5 is the nearest-neighbor distance in the two-dimensional lattice. For each NO-NO spacing and symmetry considered, a series of total-energy calculations was performed over a range of N—O bond lengths. The results were fit to parabolas to determine the equilibrium bond lengths, harmonic stretch frequencies, and ground-state energies shown in panels (a)–(c) of the figure, respectively. The calculated stretch frequencies assume that the entire N and O planes move in unison, with possible dispersion effects ignored. The horizontal dashed lines in Fig. 5 denote the experimental bond length and harmonic stretch frequency[4] for gas-phase NO.

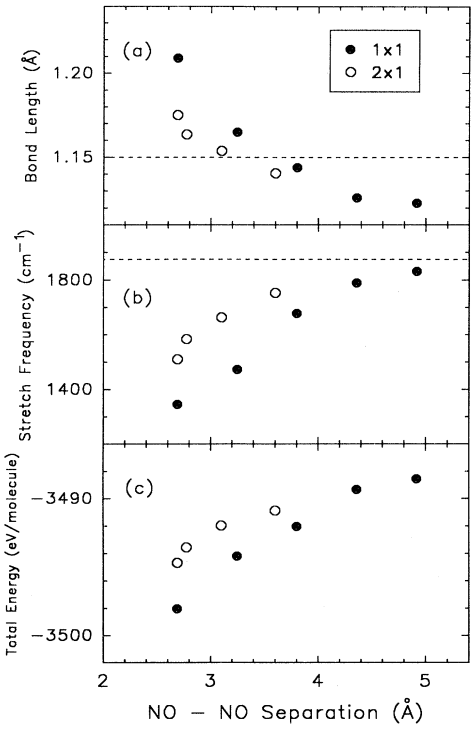

FIG. 5. Calculated (a) N—O bond lengths, (b) N-O stretch frequencies, and (c) total energies for square 1×1 (filled circles) and rectangular 2×1 (open circles) NO monolayers as a function of the nearest-neighbor NO-NO separation. Dashed lines in (a) and (b) are experimental values from Ref. 4.

As the NO-NO separation increases, the monolayer results must eventually saturate to the values the PSF method would predict for an isolated NO molecule. This saturation is already apparent in Fig. 5 at the largest separations it was practical to consider. The N—O bond length extrapolates to a value of roughly 1.12 Å, which is 2.6% below the observed value of 1.15 Å. The extrapolated N-O stretch frequency lies remarkably close to the observed frequency of 1876 cm^{-1}.

The calculated density of states for the 1×1 monolayer with a 4.9-Å NO-NO separation is shown in Fig. 6. Even at this large spacing, the interactions between molecules are strong enough to spread the NO molecular levels out into bands. The most significant banding effect occurs for the NO $2\pi^*$ states, which are the most delocalize of those shown. Each molecule contributes only one $2\pi^*$ electron, so the monolayer Fermi level lies near the bottom of the $2\pi^*$ band, which can accommodate up to four electrons per molecule. The density of states associated with this band exhibits one-dimensional singularities due to the dominance of σ interactions between $2\pi^*$ orbitals along the principal axes of the two-dimensional lattice.[17] The 1π band also exhibits such singularities, although they are smeared together in Fig. 6 because of a 0.2-eV broadening that was included in the calculations. The relative locations[73] of the bands in Fig. 6 agree very well with photoemission spectra for gaseous NO,[74] and with LDA results for an isolated NO molecule.[75] The EHT

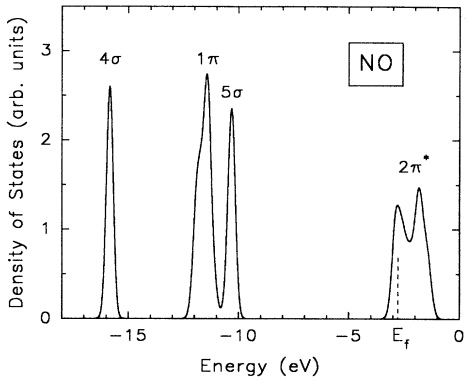

FIG. 6. Calculated density of states for a square 1×1 NO monolayer with a NO-NO separation of 4.9 Å. States are labeled by their dominant molecular-orbital component. E_F is the Fermi level, and the zero of energy is the potential infinitely far from the N side. The results are broadened by 0.2 eV.

monolayer calculations of Ref. 17, by contrast, give a much larger separation between 4σ and 1π bands (7.5 eV) and a much smaller separation between 5σ and $2\pi^*$ bands (2 eV).

With decreasing NO-NO separation, the banding effects become even more pronounced, and the total energy in Fig. 5 decreases due to delocalized metallic bonding. At some point this energy must go back up due to the Pauli repulsion between molecules, but the minimum-energy spacing is smaller than any considered here. The increased intermolecular bonding at smaller spacings causes an elongation of the N—O bond and a decrease in the N-O stretch frequency. This is consistent with bond-order-conservation arguments[76] that suggest that increased intermolecular bonding must be accompanied by decreased intramolecular bonding. The same arguments account for the differences between the 1×1 and 2×1 monolayers since each NO molecule in the former has two more nearest neighbors than in the latter. For comparisons to $p(2\times1)$ and $c(2\times2)$, $\theta=0.5$ chemisorbed systems (cf. Fig. 1), the most relevant results in Fig. 5 are those for 2×1 monolayers with the same lattice spacings as the metal surfaces (2.69–2.77 Å) and for 1×1 monolayers with spacings greater by a factor of $\sqrt{2}$ (i.e., 3.80–3.92 Å). Despite the similar densities, the NO-NO interactions are stronger in the former case because of the shorter minimum NO-NO separation. For either symmetry, however, the direct NO-NO interactions are clearly significant, and their influence on the chemisorbed systems may be difficult to separate from those of the metal.

V. CHEMISORBED SYSTEMS

PSF calculations for $p(2\times1)$, $\theta=0.5$ coverages of linear NO in twofold bridge and atop sites on Rh, Pd, and Pt (100) were performed for a range of N—O bond lengths, d_{NO}, and metal—N bond lengths, d_{MN}. The total-energy results were fit with smooth curves to determine the preferred values of these bond lengths and the force constants k_{NO} and k_{MN} associated with N—O and metal—N bond stretching, respectively.

TABLE II. Calculated N—O and metal—N bond lengths (d_{NO} and d_{MN}, respectively, in Å) and the binding-energy difference between atop and bridge (br) sites ($\Delta E_{atop\text{-}br}$, in eV/NO molecules) for $\theta=0.5$, $p(2\times1)$ coverages of linear NO on Rh, Pd, and Pt (100) surfaces. ML denotes results for a free-standing NO monolayer at the same NO-NO separation as on the corresponding metal surface.

		NO/Rh	NO/Pd	NO/Pt
d_{NO}	(ML)	1.175		1.162
	(br)	1.268	1.256	1.264
	(atop)	1.182	1.168	1.169
d_{MN}	(br)	1.795	1.772	1.832
	(atop)	1.747	1.760	1.807
$\Delta E_{atop\text{-}br}$		1.84	2.91	0.07

Table II lists the optimized bond lengths for the chemisorbed systems, together with the optimized N—O bond lengths for free-standing 2×1 NO monolayers with the same spacings as on Rh and Pt. Compared to the monolayer results, the N—O bond lengths increase slightly upon adsorption in atop sites and increase by 8–9 % upon adsorption in bridge sites. The metal—N bond lengths are also larger for bridge than atop sites. The last row in Table II lists the energy differences between the optimized atop- and bridge-site geometries. In all cases, the bridge site is preferred, with the energy difference increasing from nearly zero in Pt to nearly 3 eV/NO molecule in Pd. Although the magnitudes here may be somewhat overestimated, the predicted trend is qualitatively consistent with vibrational studies of NO, which suggest primarily bridge-site adsorption on Rh (Refs. 77–79) and Pd,[32,47,80–82] and both bridge- and atop-site adsorption on Pt.[33,83–86]

Most aspects of NO chemisorption on transition-metal surfaces are understandable within the Blyholder model,[21,71,87] which was originally developed for CO chemisorption. In this model, CO binds to metals because of σ donation from the occupied CO 5σ level to unoccupied d states and π backbonding from occupied d states to the unoccupied CO $2\pi^*$ level. Both these CO molecular orbitals have a larger amplitude on C, so the binding occurs with the C side down. NO chemisorption is very similar, although NO has one more electron than CO, which causes the $2\pi^*$ level to lie lower in energy and to be partially occupied even in an isolated molecule. NO also differs from CO in that an electron in the 5σ level is more evenly distributed throughout the molecule.[6,88] Both these differences cause π backbonding to be more important for NO than for CO chemisorption. The relative importance of σ donation is further weakened in the systems considered here by the nearly filled d bands of Rh, Pd, and Pt.

The dominance of π backbonding makes bridge-site adsorption energetically favorable in these systems. The $2\pi^*$ orbital of a NO molecule in a bridge site has more occupied metal d states of appropriate symmetry with which to interact; in addition, it couples primarily to metal d states of antibonding character, which lie closer to the Fermi level.[15] Bridge-site adsorption thus results in a greater occupancy of NO $2\pi^*$ antibonding levels, which in turn produces weaker and longer N—O bonds than atop-site adsorption. The much stronger preference for bridge sites exhibited by Pd, compared to Pt, is a consequence of the higher Fermi level, higher band filling, and narrower d band of Pd. All these effects place more occupied d states of appropriate symmetry for π backbonding closer in energy to the NO $2\pi^*$ level. The weak site preference in Pt is also due in part to its relativistic nature, which enhances σ donation to unoccupied s states, thus reducing the energy penalty for atop sites. The value of $\Delta E_{atop\text{-}br}$ for Rh is intermediate between that of Pd and Pt due to its intermediate bandwidth and a competition between the effects of Rh's higher Fermi level and lower band filling.

In contrast to NO, CO often adsorbs in atop sites on Rh (Refs. 71 and 89) as well as on Pt. This difference is consistent with the weaker π backbonding and stronger σ donation in CO discussed above. These trends are not sufficient to overcome the strong promotion of π backbonding on Pd(100), which makes bridge-site adsorption favorable even for CO.[89–91]

The present prediction that a half-monolayer of NO preferentially occupies bridge sites on Rh(100) is consistent with a previous EHT study of this system.[16] The more recent EHT calculations of Ward, Hoffmann, and Shelef,[17] however, reach a qualitatively different conclusion from the present work as to the strength of the N—O bond when chemisorbed on Pd and Pt. The calculated overlap populations in that work suggest that the N—O bond is strengthened in both bridge and atop sites on Pd and Pt (100). Here, by contrast, the predicted bond lengths in Table II show a weakening (elongation) of the N—O bond on all three metals, especially in bridge sites. The largest elongation does occur on Rh, but this may simply be due to the smaller NO-NO separation, which causes a similar trend in monolayer results. The qualitatively different EHT prediction is most likely due to the inaccurate EHT work functions in Table I; these cause the NO $2\pi^*$ electron to spill over almost completely into the Pd or Pt d band, thus increasing the N—O bond strength by depopulating an antibonding level. Clearly, in the more accurate and self-consistent PSF method, this effect does not occur to any great extent, and the NO $2\pi^*$ states, if anything, gain in occupancy.

Further similarities between the chemisorption behavior of NO on Rh, Pd, and Pt (100) are apparent from electronic structure results for the coupled systems. Figures 7 and 8 show densities of states projected on NO orbitals for optimized atop- and bridge-site geometries, respectively. The two figures differ significantly, but in both cases the results for the three different metals are nearly indistinguishable.

The low-energy 4σ peaks in Figs. 7 and 8 are largely insensitive to the adsorption site. On all three metals this peak lies below the d-band region and lies further below the Fermi level than for an isolated NO monolayer (cf. Fig. 6) because of interactions with unoccupied metal states. The 4σ peak lies lowest in the case of Pt because of the relatively strong σ donation in Pt discussed earlier. The NO 5σ-derived states are also downshifted by σ

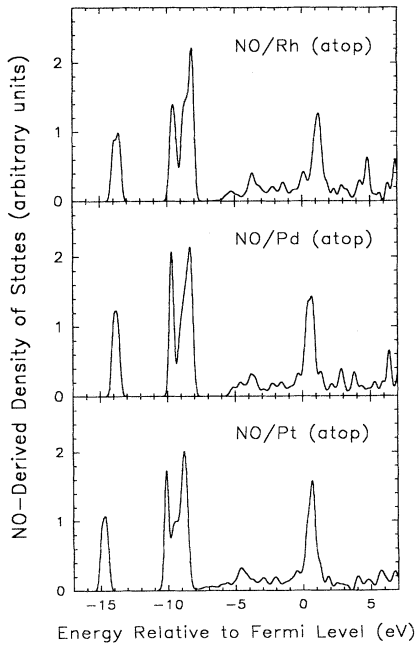

FIG. 7. Densities of states projected on NO orbitals for $\theta=0.5$, $p(2\times1)$ coverages of NO in atop sites on Rh, Pd, and Pt (100) surfaces.

donation on all three metals, with the effect being larger for atop sites. Whereas in Fig. 6 the NO 5σ states lie above the NO 1π states, the two sets of states are largely superposed in Fig. 8, and the NO 5σ states lie below the NO 1π states in Fig. 7. The other major difference between Figs. 7 and 8 occurs within ±6 eV of the Fermi level, where the states shown are derived primarily from

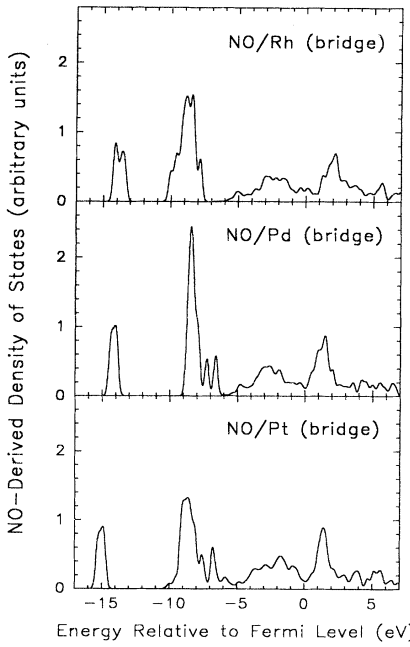

FIG. 8. Same as Fig. 7, but for bridge-site adsorption.

NO $2\pi^*$ orbitals. For atop-site adsorption in Fig. 7 there is a pronounced peak just above the Fermi level, with a much smaller density of states elsewhere in the region. For bridge-site adsorption in Fig. 8 there are two main peaks at -2 to -3 eV and at $+1$ to $+2$ eV, with the Fermi level lying near a density-of-states minimum. The two peaks are a consequence of the strong π backbonding at bridge sites, which give rise, respectively, to bonding and antibonding combinations of $2\pi^*$ orbitals and metal d states.

The calculated NO-derived states in Fig. 8 are in excellent agreement with photoemission[74,92–98] and inverse photoemission[99,100] spectra for chemisorbed NO on a variety of low-index Rh, Pd, and Pt surfaces. Photoemission spectra measured before and after NO adsorption are remarkably consistent in showing the main NO-induced features to lie between -14.8 and -14.5 eV, between -9.7 and -9.0 eV, and between -2.8 and -2.0 eV. Inverse photoemission spectra show the main NO-induced feature on Pd(100) and Pd(111) to lie between $+1.5$ and $+1.8$ eV. These features have generally been correctly identified in the experimental studies, although there has been some confusion over the appearance of $2\pi^*$ features in both occupied and unoccupied regions.[92,99] Figure 8 confirms that the NO $2\pi^*$ states are indeed responsible for both features, although the NO $2\pi^*$ states are everywhere strongly mixed with metal d orbitals. Such strong hybridization has also been found in most previous calculations for NO bonded to transition metals.[6–12,88] [Note, however, that in Fig. 7 of Ref. 17 the $2\pi^*$ states are not strongly perturbed by adsorption on Pd and Pt (100) because the EHT parametrization in that work places them too far above the Pd and Pt d bands.]

Because of the large role that vibrational spectroscopy has played in determining NO adsorption sites,[32,33,47,77–86] it is interesting to examine predictions of the present PSF method for the N-O and metal-N stretch frequencies, ν_{NO} and ν_{MN}, respectively. If one assumes that these two modes are decoupled and that the metal slab has infinite mass, the calculated force constants k_{NO} and K_{MN} mentioned at the beginning of this section yield the results in Table III. The values in parentheses include the additional effect of the mechani-

TABLE III. Calculated N-O and metal-N stretch frequencies (ν_{NO} and ν_{MN}, respectively, in cm^{-1}) for $\theta=0.5$, $p(2\times1)$ coverages of linear NO in bridge (br) and atop sites on Rh, Pd, and Pt (100) surfaces. Main entries are uncoupled frequencies, and values in parentheses include the coupling between the two modes. ML denotes results for a free-standing NO monolayer at the same NO-NO separation as on the corresponding metal surface.

		NO/Rh	NO/Pd	NO/Pt
ν_{NO}	(ML)	1509		1590
	(br)	1537 (1735)	1411 (1512)	1235 (1322)
	(atop)	1771 (2037)	1757 (2004)	1860 (2091)
ν_{MN}	(br)	691 (612)	481 (449)	420 (392)
	(atop)	856 (744)	823 (721)	823 (732)

cal coupling between these modes, calculated using the $M \rightarrow \infty$ limit of the model of Ford and Weber.[101] For comparison, the first line in Table III lists the N-O stretch frequencies for free-standing 2×1 NO monolayers with the same spacings as Rh and Pt.

The calculated N-O stretch frequencies for atop sites are significantly higher than those of either bridge sites or isolated monolayers. Recall that the monolayer frequencies are below that of gas-phase NO because of the lateral coupling between molecules. This coupling is less effective in the case of chemisorbed systems because of the much stronger interaction between each molecule and the metal (another example of a bond order conservation effect[76]). The differences between N-O stretch frequencies for bridge and atop sites are due primarily to the longer N—O bonds at bridge sites (cf. Table II). The metal-N stretch frequencies in Table III are also lower for bridge sites, although the differences compared to atop sites are too large to explain in terms of bond-length differences alone. The decrease in ν_{MN} from Rh→Pd→Pt for bridge sites is consistent with the trend in metal-N bond strengths implied by the trend in metal Fermi-level positions. The similar trend in ν_{NO} for bridge sites is counterintuitive and most likely results from differences in the amount of charge transfer and screening that occur, as well as the differences in clean metal properties discussed in Sec. III. It is clear from an examination of PSF charges and potentials that the simple orbital interaction ideas discussed throughout this section provide only a limited understanding of the self-consistent electronic structures of chemisorbed systems. Bridge-site adsorption, for example, leads to a significant preferential increase in the charge around O atoms, which can only be explained by allowing the NO orbitals themselves to adjust to changes in the electrostatic potential.

Quantitatively, the results in Table III are not sufficiently accurate to assist in the interpretation of experimental vibrational spectra.[32,33,47,77–86] The metal-N stretch frequencies, in particular, are much higher than the 200–400-cm^{-1} values usually observed for NO on Rh, Pd, and Pt. This overestimate is probably a consequence of our not allowing the metal atoms to relax; true metal-N stretching vibrations undoubtedly involve the concerted motion of several near-neighbor metal atoms together with the NO molecule. The overestimates of ν_{MN} in Table III also lead to exaggerations of the effects of the coupling between metal-N and N-O stretching modes. The predictions of $\nu_{NO} > 2000$ cm^{-1} for the coupled vibrations of atop-site adsorbates are well above the range (1650–1800 cm^{-1}) usually assigned to atop-site NO on Rh, Pd, and Pt. The prediction that 1537 $cm^{-1} < \nu_{NO} < 1735$ cm^{-1} for bridge-site NO on Rh(100) is in reasonable agreement with the experimental value of 1630 cm^{-1} for $\theta=0.5$ estimated from Ref. 77. The predicted values of ν_{NO} for bridge-bonded NO on Pd and Pt (100), on the other hand, are well below the range usually assigned to these species (1470–1700 cm^{-1}).[32,33,47]

It should be noted, of course, that the usual practice of interpreting the vibrational spectra of chemisorbed NO based on comparisons to transition-metal nitrosyl compounds has become increasingly questioned as more reliable methods for determining adsorbate structures have become available.[102] Although the present theoretical method is not sufficiently quantitative, it does serve to illustrate many of the complications that are unique to surface adsorbates: e.g., electrostatic[103] and bonding interactions between molecules, metallic screening, and competition for metal d electrons.[78] These effects are particularly important for understanding the significant shifts that occur in vibrational frequencies with increasing coverage.[78,78] Assignments based on nitrosyl compounds are also questionable because of the intrinsic differences between NO bonding and the mechanical coupling[101] between N-O stretching and other vibrational modes in compounds and on surfaces. Given the success of density-functional theory, and the LDA in particular, for calculating the vibrational properties of other systems,[104,105] we expect that the inaccuracies in the present calculations are primarily computational in nature and not due to deficiencies in the underlying theory.

VI. CONCLUDING COMMENTS

The most striking aspect of the present results is the remarkable similarity in predicted chemisorption behavior for NO on Rh, Pd, and Pt (100). All three systems exhibit similar site preferences, bond lengths, and electronic structures. With the possible exception of the stronger metal-N coupling for Rh in Table III, there is very little in these results to suggest why Rh is a more effective catalyst for NO reduction than Pd or Pt. The situation is certainly more complicated than the EHT conclusion of Ref. 17 that the N—O bond is weakened on Rh, but strengthened on Pd and Pt. The present calculations do not support this conclusion. They do, however, demonstrate the superiority of the PSF-LDA approach over that of EHT for calculating properties that are currently testable against experimental data (e.g., clean metal work functions and bandwidths and adsorbate electronic structures).

Thus, while we are encouraged by the success of the PSF-LDA description of NO chemisorption, the present results do not succeed in explaining why Rh is particularly well suited for NO reduction in automative catalysts. Of course, any model based on single-crystal surfaces cannot possibly treat the full complexities of practical supported-metal catalysts in which the supports themselves (in this case, alumina and other ingredients) interact with highly dispersed metal clusters. NO reduction, in particular, is well known to be structure sensitive, meaning that its behavior can be quite different in the presence of single-crystal surfaces and supported-metal particles.[106] Even for single-crystal surfaces, however, the present results do not explain why NO dissociates more easily on Rh than on Pd or Pt;[70] to understand this, one would need to perform additional calculations for bent NO and for atomic N and O adsorbates. Such calculations would be cumbersome with the present approach, but may soon be tractable with one of the first-principles (LDA) molecular-dynamics methods that is being developed to treat transition-metal systems.[107,108] Such methods would also be better suited for further study of the NO-NO coupling mechanism proposed in

Ref. 17. As this mechanism would naturally explain the strong selectivity of Rh-based catalysts for N_2 instead of NH_3 products,[5] it deserves to be tested with a more sophisticated method than EHT.

ACKNOWLEDGMENTS

We have benefited greatly from discussions with G. W. Graham, R. Hoffmann, R. V. Kasowski, and M. Shelef.

*Present address: Department of Physics, National Sun Yat-Sen University, Kaohsiung, Taiwan 80424, Republic of China.

[1]J. T. Kummer, J. Phys. Chem. **90**, 4747 (1986).

[2]J. T. Kummer, Prog. Energ. Combust. Sci. **6**, 177 (1980).

[3]K. C. Taylor, in *Catalytic Chemistry of Nitrogen Oxides,* edited by R. L. Klimisch and J. G. Larson (Plenum, New York, 1975), p. 173.

[4]A recent review of much of the literature is given by G. B. Richter-Addo and P. Legzdins, *Metal Nitrosyls* (Oxford University Press, New York, 1992).

[5]M. Shelef and G. W. Graham, Catal. Rev. Sci. Eng. **36**, 433 (1994).

[6]I. P. Batra and C. R. Brundle, Surf. Sci. **57**, 12 (1976).

[7]D. T. Clark, B. J. Cromarty, and A. Sgamellotti, Chem. Phys. Lett. **68**, 420 (1979).

[8]A. Schichl and N. Rösch, Surf. Sci. **137**, 261 (1984).

[9]C. W. Bauschlicher, Jr. and P. S. Bagus, J. Chem. Phys. **80**, 944 (1984).

[10]P. S. Bagus, C. J. Nelin, and Ph. Avouris, J. Vac. Sci. Technol. A **5**, 701 (1987).

[11]M. Fernández-García, J. C. Conesa, and F. Illas, Surf. Sci. **280**, 441 (1993).

[12]G. W. Smith and E. A. Carter, J. Phys. Chem. **95**, 2327 (1991).

[13]J. Sauer, Chem. Rev. **89**, 199 (1989).

[14]G. te Velde and E. J. Baerends, Chem. Phys. **177**, 399 (1993).

[15]S.-S. Sung, R. Hoffmann, and P. A. Thiel, J. Phys. Chem. **90**, 1380 (1986).

[16]D. L. Vuçković, S. A. James, and R. Hoffmann, Langmuir **6**, 732 (1990).

[17]T. R. Ward, R. Hoffmann, and M. Shelef, Surf. Sci. **289**, 85 (1993).

[18]T. R. Ward, P. Alemany, and R. Hoffmann, J. Phys. Chem. **97**, 7691 (1993).

[19]W. F. Egelhoff, Jr., in *The Chemical Physics of Solid Surfaces and Heterogeneous Catalysis,* edited by D. A. King and D. P. Woodruff (Elsevier, Amsterdam, 1982), Vol. 4, p. 397.

[20]K. C. Taylor, Catal. Rev. Sci. Eng. **35**, 457 (1993).

[21]R. Hoffmann, Rev. Mod. Phys. **60**, 601 (1988).

[22]As one example, compare M. Kertesz and R. Hoffmann, J. Solid State Chem. **54**, 313 (1984); S. Fahy, S. G. Louie, and M. L. Cohen, Phys. Rev. B **34**, 1191 (1986).

[23]R. V. Kasowski, M.-H. Tsai, T. N. Rhodin, and D. D. Chambliss, Phys. Rev. B **34**, 2656 (1986).

[24]R. V. Kasowski, T. Rhodin, and M.-H. Tsai, Appl. Phys. A **41**, 61 (1986).

[25]L. Hedin and B. I. Lundquist, J. Phys. C **4**, 2064 (1971).

[26]O. K. Anderson, Phys. Rev. B **12**, 3060 (1975).

[27]G. B. Bachelet, D. R. Hamann, and M. Schlüter, Phys. Rev. B **26**, 4199 (1982).

[28]M.-H. Tsai, J. D. Dow, and R. V. Kasowski, Phys. Rev. B **38**, 2176 (1988).

[29]R. V. Kasowski, M.-H. Tsai, and J. D. Dow, Phys. Rev. B **41**, 8949 (1990).

[30]R. V. Kasowski, M.-H. Tsai, S. T. Chui, and J. D. Dow, Phys. Rev. B **46**, 10017 (1992).

[31]P. Ho and J. M. White, Surf. Sci. **137**, 103 (1984).

[32]S. W. Jorgensen, N. D. C. Canning, and R. J. Madix, Surf. Sci. **179**, 322 (1987).

[33]G. Pirug, H. P. Bonzel, H. Hopster, and H. Ibach, J. Chem. Phys. **71**, 593 (1979).

[34]M.-H. Tsai (unpublished).

[35]K. Kambe, Z. Naturforsch **22**, 322 (1967); **22**, 422 (1967); **23**, 1280 (1968).

[36]J. B. Pendry, *Low Energy Electron Diffraction* (Academic, London, 1974), p. 137.

[37]E. Wimmer, H. Krakauer, M. Weinert, and A. J. Freeman, Phys. Rev. B **24**, 864 (1981).

[38]Our rule of thumb, based on considerations discussed in Ref. 23, is to use a cutoff that is the larger of $7/r_d$, where r_d is the smallest radius in the problem for an element with d orbitals, or $5/r_{sp}$, where r_{sp} is the smallest radius in the problem for an element without d orbitals.

[39]J. Emsley, *The Elements* (Clarendon, Oxford, 1989).

[40]D. G. Castner, B. A. Sexton, and G. A. Somorjai, Surf. Sci. **71**, 519 (1978).

[41]J. Quinn, Y. S. Li, D. Tian, H. Li, F. Jona, and P. M. Marcus, Phys. Rev. B **42**, 11 348 (1990).

[42]W. Oed, B. Dötsch, L. Hammer, K. Heinz, and K. Müller, Surf. Sci. **207**, 55 (1988).

[43]P. J. Feibelman and D. R. Hamann, Surf. Sci. **234**, 377 (1990).

[44]L. Morrison, D. M. Bylander, and L. Kleinman, Phys. Rev. Lett. **71**,1083 (1993).

[45]A. M. Begley, S. K. Kim, F. Jona, and P. M. Marcus, Phys. Rev. B **48**, 12 326 (1993).

[46]B. Piveteau, D. Spanjaard, and M. C. Desjonquéres, Phys. Rev. B **49**, 8402 (1994).

[47]C. Nyberg and P. Uvdal, Surf. Sci. **204**, 517 (1988).

[48]U. von Barth and L. Hedin, J. Phys. C **5**,1629 (1982).

[49]K. C. Hass, M.-H. Tsai, and R. V. Kasowski (unpublished).

[50]S. L. Cunningham, Phys. Rev. B **10**, 4988 (1974).

[51]D. D. Johnson, Phys. Rev. B **38**, 12 807 (1988).

[52]O. K. Anderson, Phys. Rev. B **2**, 883 (1970).

[53]V. L. Moruzzi, J. F. Janak, and A. R. Williams, *Calculated Electronic Properties of Metals* (Pergamon, New York, 1978).

[54]D. A. Papaconstantopoulos, *Handbook of the Band Structure of Elemental Solids* (Plenum, New York, 1986).

[55]J. G. Gay, J. R. Smith, F. J. Arlinghaus, and T. W. Capehart, Phys. Rev. B **23**, 1559 (1981).

[56]J. G. Gay, J. R. Smith, and F. J. Arlinghaus, Phys. Rev. B **25**, 643 (1982).

[57]P. J. Feibelman and D. R. Hamann, Phys. Rev. B **28**, 3092 (1983).

[58]S. Wilke, D. Hennig, and R. Löber, Phys. Rev. B **50**, 2548

(1994).
[59]J. T. Waber and D. T. Cromer, J. Chem. Phys. **42**, 4116 (1965).
[60]P. Pyykkö, Chem. Rev. **88**, 563 (1988).
[61]R. Smoluchowski, Phys. Rev. **60**, 661 (1941).
[62]M. Methfessel, D. Hennig, and M. Scheffler, Phys. Rev. B **46**, 4816 (1992).
[63]V. Fiorentini, M. Methfessel, and M. Scheffler, Phys. Rev. Lett. **71**, 1051 (1993).
[64]G. B. Fisher (unpublished), cited in Ref. 55.
[65]H. B. Michaelson, J. Appl. Phys. **48**, 4729 (1977).
[66]H. Hochst, M. K. Kelly, and G. B. Fisher (unpublished), cited in Ref. 43.
[67]A. M. Bradshaw (unpublished), cited in Ref. 56.
[68]P. J. Feibelman and D. R. Hamann, Phys. Rev. Lett. **52**, 61 (1984).
[69]See, for example, the discussion in Y.-T. Wong and R. Hoffmann, J. Phys. Chem. **95**, 859 (1991), which attempts to rationalize the predicted EHT ordering of Pd and Pt Fermi levels.
[70]G. Brodén, T. N. Rhodin, C. Bruckner, R. Benbow, and Z. Hurych, Surf. Sci. **59**, 593 (1976).
[71]R. A. van Santen, *Theoretical Heterogeneous Catalysis* (World Scientific, Singapore, 1991), Sec. 2.8.
[72]M. H. Cohen, M. V. Ganduglia-Pirovano, and J. Kudrnovský, Phys. Rev. Lett. **72**, 3222 (1994).
[73]The zero of energy in Fig. 6 is set by the potential infinitely far from the monolayer on the N side. The calculations give the incorrect sign for the NO dipole moment, with the O end negatively charged, presumably because of NO-NO interactions. (References 23 and 24 discuss the same problem for CO.) The potential infinitely far from the O side of the monolayer considered in Fig. 6 is approximately +0.8 eV.
[74]H. P. Bonzel and G. Pirug, Surf. Sci. **62**, 45 (1977).
[75]R. Ramprasad, K. C. Hass, and W. F. Schneider (unpublished).
[76]E. Shustorovich, Adv. Catal. **37**, 101 (1990).
[77]J. S. Villarrubia and W. Ho, J. Chem. Phys. **87**, 750 (1987).
[78]T. W. Root, G. B. Fisher, and L. D. Schmidt, J. Chem. Phys. **85**, 4679 (1986).
[79]G. Cautero, C. Astaldi, P. Rudolf, M. Kiskinova, and R. Rosei, Surf. Sci. **258**, 44 (1991).
[80]M. Bertolo and K. Jacobi, Surf. Sci. **226**, 207 (1990).
[81]R. Raval, M. A. Harrison, S. Haq, and D. A. King, Surf. Sci. **294**, 10 (1993).
[82]P. J. Chen and D. W. Goodman, Surf. Sci. Lett. **297**, L93 (1993).
[83]H. Ibach and S. Lehwald, Surf. Sci. **76**, 1 (1978).
[84]J. L. Gland and B. A. Sexton, Surf. Sci. **94**, 355 (1980).
[85]R. J. Gorte and J. L. Gland, Surf. Sci. **102**, 348 (1981).
[86]B. E. Hayden, Surf. Sci. **131**, 419 (1983).
[87]G. Blyholder, J. Phys. Chem. **68**, 2772 (1964).
[88]G. Doyen and G. Ertl, Surf. Sci. **69**, 157 (1977).
[89]A. Goursot, I. Papai, and D. R. Salahub, J. Am. Chem. Soc. **114**, 7452 (1992).
[90]A. B. Anderson and Md. K. Awad, J. Am. Chem. Soc. **107**, 7854 (1985).
[91]G. Pacchioni and P. S. Bagus, J. Chem. Phys. **93**, 1209 (1990).
[92]H. Conrad, G. Ertl, J. Küppers, and E. E. Latta, Surf. Sci. **65**, 235 (1977).
[93]R. J. Baird, R. C. Ku, and P. Wynblatt, Surf. Sci. **97**, 346 (1980).
[94]A. Morgante, D. Cvetko, A. Santoni, K. C. Prince, V. R. Dhanak, G. Comelli, and M. Kiskinova, Surf. Sci. **285**, 227 (1993).
[95]S. Sugai, H. Watanabe, T. Kioka, H. Miki, and K. Kawasaki, Surf. Sci. **259**, 109 (1991).
[96]S. Sugai, K. Takeuchi, T. Ban, H. Miki, K. Kawasaki, and T. Kioka, Surf. Sci. **282**, 67 (1993).
[97]S. Sugai, K. Shimizu, H. Watanabe, H. Miki, K. Kawasaki, and T. Kioka, Surf. Sci. **287/288**, 455 (1993).
[98]K. C. Prince, A. Santoni, A. Morgante, and G. Comelli, Surf. Sci. **317**, 397 (1994).
[99]J. Rogozik, J. Küppers, and V. Dose, Surf. Sci. **148**, L653 (1984).
[100]P. D. Johnson and S. L. Hulbert, Phys. Rev. B **35**, 9427 (1987).
[101]G. W. Ford and W. H. Weber, Surf. Sci. **129**, 123 (1983).
[102]L. D. Mapledoran, A. Wander, and D. A. King, Chem. Phys. Lett. **208**, 409 (1993).
[103]M. Scheffler, Surf. Sci. **81**, 562 (1979).
[104]B. G. Johnson, P. M. W. Gill, and J. A. Pople, J. Chem. Phys. **98**, 5612 (1993).
[105]W. Windl, K. Karch, P. Pavone, O. Schütt, D. Strauch, W. H. Weber, K. C. Hass, and L. Rimai, Phys. Rev. B **49**, 8764 (1994).
[106]S. H. Oh, G. B. Fisher, J. E. Carpenter, and D. W. Goodman, J. Catal. **100**, 360 (1986).
[107]M.-H. Tsai and K. C. Hass (unpublished).
[108]S. H. Yang, D. A. Drabold, J. B. Adams, P. J. Ordejon, and K. M. Glassford (unpublished).